23rd International Conference
ENGINEERING MECHANICS 2017
Svratka, Czech Republic, 15 – 18 May 2017

EXPLICIT DYNAMIC FINITE ELEMENT ANALYSIS OF A FIRING PIN ASSEMBLY

D. Mochar[*], D. Gabriel[*], J. Masák[*], J. Kopačka[*], R. Kolman[*], J. Plešek[*]
P. Hynek[*], J. Vtípil[**]

Abstract: *In this paper, explicit dynamic finite element analysis of a firing pin assembly was performed. Two different geometries of the firing pin were considered using the finite element software PMD and Abaqus. For both variants there was evaluated a stress distribution at the critical point of a tested component, that is going to be later used for a fatigue analysis of the firing pin.*

Keywords: Firing pin, Explicit dynamic analysis, FEM, Fatigue.

1. Introduction

A firing pin is a central structural element of any firearm. Therefore, it is crucial to secure its correct operation, which is necessary for functionality of a complete firearm. In some cases during real construction process the stress damage is cumulated in the critical point and can lead to a fatigue fracture. Due to the nature of the firing pin, especially its low weight and high impact forces, it is necessary to take into account the stress wave propagation in the structure (Mochar, 2016). In this paper, time distributions of kinematic and stress quantities in the critical point of firing pin was calculated in the dynamic finite element analysis (FEA). Two different geometries of the firing pin were considered using the finite element software PMD (VAMET LLC. 2013) and Abaqus. Finally, the rough estimation of lifetime of both variants was determined.

2. Finite element analysis

CAD model of a firing pin is plotted in Fig. 1. Two geometries of firing pin were considered varying in the length between the impact surface and critical point of the firing pin (tip of the radius R50) denoted as R50 – 42.0 mm (var. A) and R50 – 44.7 mm (var. B).

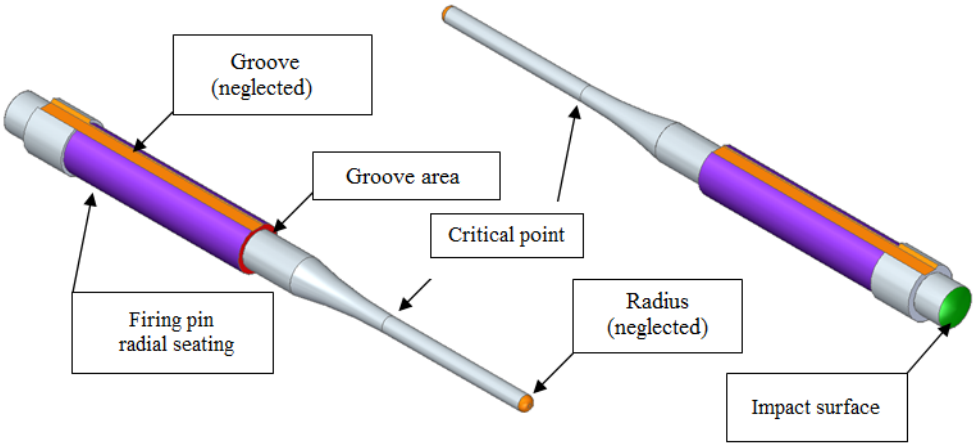

Fig. 1: CAD model of a firing pin.

[*] Institute of Thermomechanics of the CAS, v. v. i., Dolejškova 5, 182 00 Prague, Czech Republic
[**] Česká zbrojovka, a.s., Svatopluka Čecha 1283, 688 27 Uherský Brod, Czech Republic

The firing pin is radially imposed on the surface denoted as „Firing pin radial seating“. The axial movement of the firing pin with prescribed initial velocity v = 9 m/s is excited by hit a hammer on the impacted surface. After travelling a distance of 2 mm the firing pin hits the backstop.

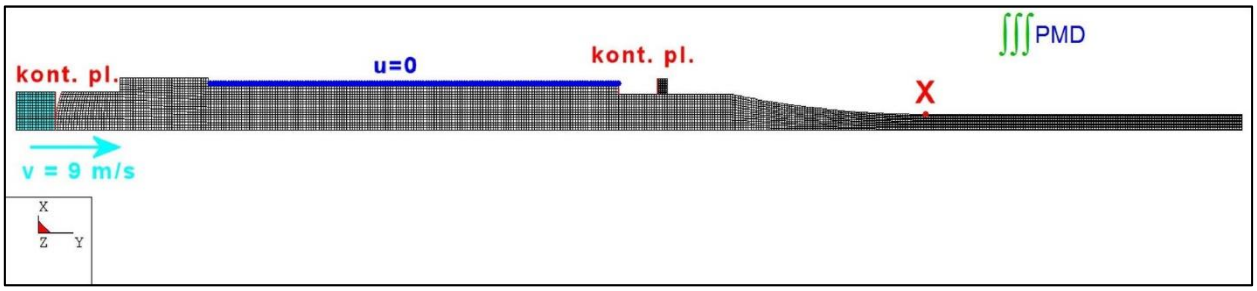

Fig. 2: Finite element model of the firing pin including hammer and backstop.

For both variants of the firing ring the material properties were considered linear elastic with Young‘s modulus $E = 1.98 \cdot 10^5$ MPa, Poisson’s ratio ν = 0.28 and density $\rho = 7\,850\ kg \cdot m^{-3}$. It corresponds to the speed of longitudinal waves $c_L = 5\,653.3\ m/s$. Young‘s modulus of rigid hammer and rigid backstop were chosen two orders of magnitude greater than modulus of the firing pin, i.e. $E = 1.98 \cdot 10^7$ MPa; Poisson’s ratio was the same value as for the firing pin. Since correct transmission of prescribed initial velocity of firing pin v = 9 m/s the fictitious density of hammer was calculated so its weight was the same as the firing pin:

- var. A - volume of firing pin 677.262 mm^3, volume of hammer 25.133 mm^3, density of hammer 211 537.121 $kg \cdot m^{-3}$,
- var. B – volume of firing pin 701.131 mm^3, volume of hammer 25.133 mm^3, density of hammer 218 992.462 $kg \cdot m^{-3}$.

The problem was treated as axisymmetric one discretized by four-node quadrilateral elements with 2 x 2 integration. Based on the recommendation of a choice of permissible dimensionless wavelength for linear and quadratic serendipity finite element meshes to supress dispersion error (Kolman et al., 2013), the length of elements was set $H = 1.2 \cdot 10^{-4}\ m$ at the most. The hammer and backstop were modelled as a rigid body. The finite element model of the firing pin including hammer and backstop is shown in Fig. 2, where the location of the critical point of the firing pin is marked by X. Note that axial groove and radius on the tip of the firing pin are neglected in the finite element model. Furthermore, 3D model was also considered in the Abaqus containing eight-node linear elements with reduced integration (C3D8R elements). The number of nodes and elements of 2D and 3D models including hammer and backstop for both geometric variants are shown in Tab. 1.

Tab. 1: Number of nodes and elements of 2D and 3D models including hammer and backstop for geometric variants A and B.

	Var. A – 42.0 mm		Var. B – 44.7	
	nodes	elements	nodes	elements
Firing pin 2D model	7 885	7 396	7 810	7 326
Hammer 2D model	225	196	225	169
Backstop 2D model	117	96	117	96
Firing pin 3D model	58 240	62 982	58 432	63 191
Hammer 3D model	2 016	2 410	2 016	2 410
Backstop 3D model	1 280	1 728	1 280	1 728

The explicit contact-impact analysis of the firing pin was performed for variants A and B. For direct integration of the equations of motion the central difference method with the diagonal mass matrix was used. In PMD and Abaqus calculation the time step was set carefully to $\Delta t = 10^{-9}$ s and the stability of

the integration process was ensured by energy balance monitoring (Kolman at al., 2016). The impact response was calculated for $t = 4.0 \cdot 10^{-4}$s.

The influence of the penalty parameter ξ on the accuracy of the numerical solution was studied in PMD calculation for penalty-based contact algorithm (Gabriel et al., 2004). The results were compared with the Abaqus software, where the penalty was set automatically. Quite a good agreement between PMD and Abaqus was achieved for the penalty parameter $\xi = 10^{15}\ N \cdot m^{-3}$.

3. Results

The results of explicit contact-impact analysis of the firing pin for variant A and variant B are summarized in Tab. 2 and Tab. 3, respectively for PMD and Abaqus calculations. The maximum and minimum values of axial stress in the tip of radius R50 of firing pin are presented including the instant of time when those extremes were occurring. For illustration time distribution of the axial stress in the tip of radius R50 of firing pin is plotted in Fig. 3 for variant A.

Tab. 2: Extremes of axial stresses in the critical point–variant A.

	Abaqus 2D	Abaqus 3D	PMD 2D
S_{yy} max [MPa]	818	810	729
time of occurrence [s]	$3.42 \cdot 10^{-4}$	$3.32 \cdot 10^{-4}$	$3.54 \cdot 10^{-4}$
S_{yy} min [MPa]	-853	-838	-916
time of occurrence [s]	$2.77 \cdot 10^{-4}$	$2.67 \cdot 10^{-4}$	$2.66 \cdot 10^{-4}$

Tab. 3: Extremes of axial stresses in the critical point–variant B

	Abaqus 2D	Abaqus 3D	PMD 2D
S_{yy} max [MPa]	1 119	1 132	1 128
time of occurrence [s]	$2.98 \cdot 10^{-4}$	$2.99 \cdot 10^{-4}$	$2.98 \cdot 10^{-4}$
S_{yy} min [MPa]	-1 190	-1 109	-1 156
time of occurrence [s]	$3.64 \cdot 10^{-4}$	$3.65 \cdot 10^{-4}$	$3.64 \cdot 10^{-4}$

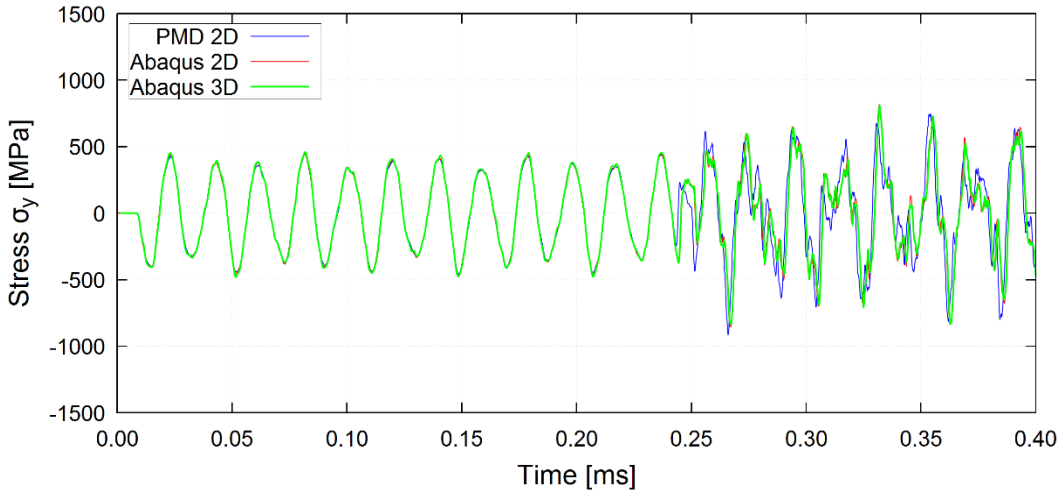

Fig. 3: Time distribution of axial stresses in the critical point–variant A.

After the evaluation of time distribution of axial stresses had been determined, the lifetime of those variants was roughly estimated using Wöhler´s curve approximation power relation. The parameters w and C of power form ($\sigma_a^w \cdot N = C$) were chosen for high-strength steel. Since the progress of this tension is almost symmetrically changing the amplitude tension σ_a is being determined as difference between

maximum and minimum value of axis tension. One cycle of burden N is simple taken as an idle shot. The comparisons of lifetime of both variants is plotted in Fig. 4.

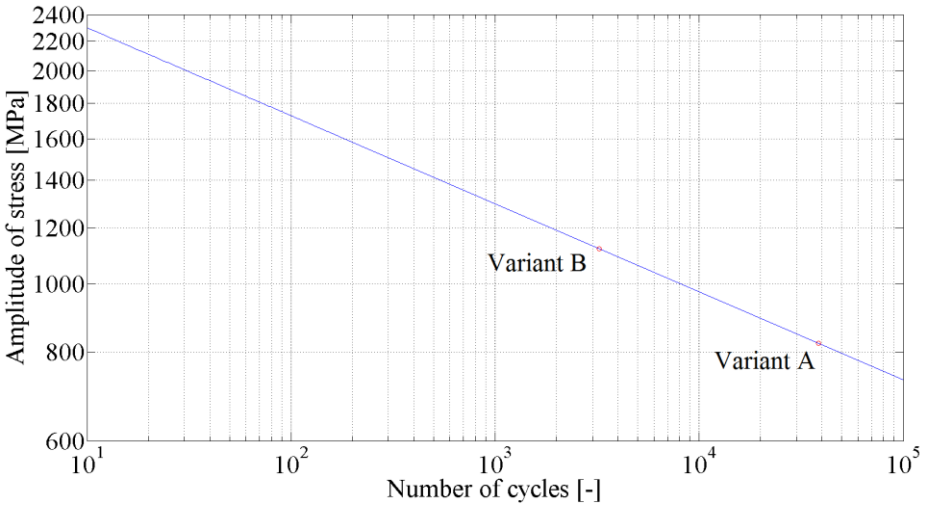

Fig. 4: Wohler's curve for comparison of lifetime of variants A and B.

4. Conclusion

After the impact of the hammer the stress waves of the sinusoidal character propagates throw the firing pin. This phenomenon stands during travelling distance of 2 mm until the firing pin hits backstop in time $t = 2.54 \cdot 10^{-4}\ s$. At this moment stress waves propagation rapidly changes due to contact condition, which significantly influences resulting stresses in the firing pin. Based on the comparison of both variants it can be concluded that variant A is more favourable where maximum reduced stress value was 917 MPa. For variant B this value was five times exceeded and the maximum reduced stress reached the maximum value 1192 MPa. Thus, the maximum difference of reduced stress between variant A and B was 275 MPa. Finally, rough lifetime estimation was done for both variants. It was demonstrated that variant A of the firing pin should be more resistant to fatigue fracture. This conclusion will be validated by experimental measurements during shooting tests with the real firearms in the future.

Acknowledgements

This work was supported by the Technology Agency of the Czech Republic under grant No TH01010772 within institutional support RVO:61388998 and the Centre of Excellence for Nonlinear Dynamic Behaviour of Advanced Materials in Engineering CZ.02.1.01/0.0/0.0/15 003/0000493 (Excellent Research Teams) in the framework of Operational Programme Research, Development and Education.

References

Gabriel, D., Plešek, J. and Ulbin, M. (2004) Symmetry preserving algorithm for large displacement frictionless contact by the pre-discretization penalty method. International Journal for Numerical Methods in Engineering 61(15): 2615-2638.

Kolman, R., Plešek, J., Červ, J., Okrouhlík, M. and Pařík, P. (2016) Temporal-spatial dispersion and stability analysis of finite element method in explicit elastodynamics. International Journal for Numerical Methods in Engineering 106(2), 113-128.

Kolman, R., Plešek J., Okrouhlík, M. and Gabriel, D. (2013) Grid dispersion analysis of plane square biquadratic serendipity finite elements in transient elastodynamics. International Journal for Numerical Methods in Engineering 96(1), 1-28.

Mochar, D. (2016) Explicit dynamic FE analysis of a firing pin assembly. Diploma thesis. CTU in Prague (in Czech).

VAMET LLC. (2013) PMD version f77.11; http://www.pmd-fem.com/.